



## **SiC-TiC nanocomposite for bulk solar absorbers applications: Effect of density and surface roughness on the optical properties**

Hélène Arena, Moustapha Coulibaly, Audrey Soum-Glaude, Alban Jonchere, Adel Mesbah, Guilhem Arrachart, Nicolas Pradeilles, Marion Vandenhende, Alexandre Maitre, Xavier Deschanel

### **► To cite this version:**

Hélène Arena, Moustapha Coulibaly, Audrey Soum-Glaude, Alban Jonchere, Adel Mesbah, et al.. SiC-TiC nanocomposite for bulk solar absorbers applications: Effect of density and surface roughness on the optical properties. *Solar Energy Materials and Solar Cells*, 2019, 191, pp.199-208. 10.1016/j.solmat.2018.11.018 . hal-02001098

**HAL Id: hal-02001098**

**<https://hal.umontpellier.fr/hal-02001098>**

Submitted on 3 Dec 2020

**HAL** is a multi-disciplinary open access archive for the deposit and dissemination of scientific research documents, whether they are published or not. The documents may come from teaching and research institutions in France or abroad, or from public or private research centers.

L'archive ouverte pluridisciplinaire **HAL**, est destinée au dépôt et à la diffusion de documents scientifiques de niveau recherche, publiés ou non, émanant des établissements d'enseignement et de recherche français ou étrangers, des laboratoires publics ou privés.

# SiC-TiC nanocomposite for bulk solar absorbers applications:

## Effect of density and surface roughness on the optical properties

Hélène Aréna<sup>1\*</sup>, Moustapha Coulibaly<sup>1</sup>, Audrey Soum-Glaude<sup>2</sup>, Alban Jonchère<sup>1</sup>, Adel Mesbah<sup>1</sup>,  
Guilhem Arrachart<sup>1</sup>, Nicolas Pradeilles<sup>3</sup>, Marion Vandenhende<sup>3</sup>, Alexandre Maitre<sup>3</sup>, and Xavier  
Deschanel<sup>1</sup>

<sup>1</sup> ICSM, CEA, CNRS, ENSCM, Univ. Montpellier, Marcoule, 30207 Bagnols-sur-Cèze, France

[helene.arena@cea.fr](mailto:helene.arena@cea.fr)

[xavier.deschanel@cea.fr](mailto:xavier.deschanel@cea.fr)

<sup>2</sup> PROMES-CNRS, UPR 8521, 7 rue du Four Solaire 66120 Font-Romeu Odeillo Via, France

<sup>3</sup> IRCER, UMR CNRS 7315, 87068 Limoges, France

Keywords: SiC ; TiC ; Concentrated Solar Power ; selectivity ; density ; roughness

### Abstract

In this study, the potential of SiC-TiC nano-composites as solar absorbers has been studied. For solar thermal applications, materials with high solar absorptance and low emittance are ideally sought for (spectral selectivity). A semi-molecular sol-gel synthesis route leading to nanometric homogenous composites was described. The resulting SiC-TiC nanocomposite powder was sintered at different temperatures to produce samples with various relative densities (from 57 to 96 %). The samples morphology and composition were characterised by several techniques including Scanning Electron Microscopy (SEM), Energy-Dispersive X-Ray Spectroscopy (EDX), X-Ray Diffraction (XRD), carbon and oxygen elemental analyses. The link between the surface roughness and the relative density was precised and the effects on the optical properties (0.25 to 25  $\mu\text{m}$  wavelength range) were studied. Comparisons were made with pure SiC and pure TiC samples with various relative densities. Overall, the sample emittance was found to strongly decrease with the increase in the relative density, leading to a great increase in the spectral selectivity, despite a little decrease in the solar absorptance. The TiC-SiC composite has an intermediate reflectance compared to the pure SiC and the pure TiC samples. With an absorptance of 0.76, an emittance of 0.44 and a selectivity of 1.74, the denser SiC-TiC could be a good candidate for bulk solar applications.

## 34 1. Introduction

35

36 The development of a sustainable, efficient and renewable energy power is a great challenge for our  
37 generation. In this context, particular attention is given to concentrating solar power (CSP) as it is a  
38 promising technology to improve the efficiency of the solar-to-electricity conversion [1, 2]. In this  
39 system, the absorber plays a key role by transferring the energy from solar radiation to a heat transfer  
40 fluid (HTF), which will be used in a thermodynamical cycle to produce electricity. However,  
41 because of thermal losses (by radiation, conduction and convection), the energy received by the  
42 absorber is not completely transferred to the HTF. As the operating temperature of the absorber is  
43 high (up to 1000°C), the main energy losses are due to thermal radiation. Indeed, when the absorber  
44 is heated, it can behave like a blackbody and emit radiation in the infrared wavelength region  
45 towards its environment. To maximize the energy efficiency, the absorber should be spectrally  
46 selective: absorbing a maximum of energy in the solar spectrum wavelength region (0.25 – 2.5  $\mu\text{m}$ ),  
47 while having a low thermal emittance in the IR region (above 2.5  $\mu\text{m}$ ), so that thermal re-radiation  
48 losses by the heated absorber are kept low [3-6]. In addition to be spectrally selective, the material  
49 constituting the absorber should be resistant to the extreme operating conditions under concentrated  
50 solar irradiation (high temperatures, oxidative/corrosive atmospheres, thermal cycles, etc.).

51

52 Nowadays, one of the materials commonly used as high temperature absorber is silicon carbide,  
53 because of its high oxidation resistance, its good mechanical properties and high sunlight  
54 absorptance [7]. However, SiC is not spectrally selective as it has a high spectral emittance [8, 9].  
55 Transition metal carbides, nitrides and borides of column IV have been subject of many  
56 investigations due to their inherent spectral selectivity [10-24]. Among these materials, titanium  
57 carbide could be a good candidate because it is spectrally selective and it has good mechanical  
58 properties. However, it also has a low resistance to oxidation [25-32]. Previous studies showed that  
59 the combination of SiC and TiC in a nanocomposite material could be a good solution to obtain a  
60 material that is spectrally selective as well as resistant to oxidation [33].

61 The literature reports the combination of SiC and TiC in a composite structure to produce materials  
62 with higher relative density and improved mechanical properties (fracture toughness, Vickers  
63 hardness), thermal and electrical conductivity [34-44]. These properties are required for the absorber  
64 material as it will endure extreme operating conditions.

65

66 Several parameters have an impact on the optical properties of the materials.

67 First, the apparent density of the material leads to changes in the optical properties of the samples.

68 The apparent density results from the process used for the material elaboration and corresponds to

69 porosity in the range of a few micrometers. Several studies indicate that the denser the material, the  
70 higher the reflectance in the whole range of wavelengths. Dense materials have a little lower  
71 absorptance ( $\alpha$ ) but above all a lower emittance ( $\epsilon$ ), thus a higher spectral selectivity which is  
72 defined as the ratio  $\alpha/\epsilon$  [19, 20, 23, 45-47].

73 Second, the surface roughness increases the absorptance of radiations in the range of wavelength  
74 lower than the average size of the holes and scratches (a few nanometers to a few hundred  
75 nanometers) [5, 6, 20, 23, 46-50]. For example, the surface patterning of zirconium boride samples  
76 by femtolaser led to better absorptance but also to higher emittance [48, 49]. The increase in the  
77 absorptance and in the emittance with the surface roughness was also noticed for SiC and TiC  
78 samples, in a preliminary study reported in Supplementary Information 1.

79

80 In most studies concerning the optical properties of UHTCs (Ultra-High Temperature Ceramics),  
81 densified or porous samples are obtained from commercial powders. To produce composites, several  
82 powders are generally mixed and sintered together. However, mechanical mixing generally induces  
83 inhomogeneities and sometimes impurities in the final composite. In the conventional process, TiC  
84 and SiC are usually synthesized by the carbothermal reduction of  $\text{TiO}_2$  or  $\text{SiO}_2$  with carbon black.  
85 This reaction requires high temperature (1800 – 2200°C), long reaction time (10 – 24h) and often  
86 leads to coarse-grained powders [51-53]. With nano-sized particles, the temperature (and/or time)  
87 needed for carbothermal reduction would decrease [54-58]. In addition, working with nano-sized  
88 materials would improve the homogeneity of the final products and lead to an intimate mixture of  
89 SiC and TiC particles.

90 Molecular routes were proposed to create proximity between the metal and the carbon source by  
91 bonding them into the same molecule. This procedure was successfully applied to SiC [59] but did  
92 not lead to a complete carbothermal reduction for TiC and SiC-TiC composites [60-62]. In addition,  
93 this route is complex and implies a thorough control of the synthesis conditions. Another way to  
94 create proximity would be to trap the carbon source in the network of a polymer material by a sol-gel  
95 process, before the carbothermal reduction. This route was applied to produce TiC, ZrC-SiC and  
96 TiC-SiC materials [63-65]. The co-condensation of the two alkoxide precursors leads to  
97 interpenetrated networks of the two oxides with enclosed carbon source particles. The carbothermal  
98 reduction produced a homogenous nanocomposite with a good repartition of both carbides and small  
99 size crystallites [66-68]. Sucrose is an interesting carbon source as it is cheap and highly soluble in  
100 several media, it was successfully used by several authors [33, 56, 57, 69, 70].

101

102 In this paper, we propose to associate SiC with TiC in a nanocomposite material for high temperature  
103 bulk solar absorber applications. We present a synthesis route where the two metal oxide precursors

104 copolymerize, in the presence of sucrose as the carbon source, leading to an intimate mixture. In  
105 order to improve the optical and mechanical properties, the resulting powders were sintered by Spark  
106 Plasma Sintering (SPS) to produce materials with various densities. The samples morphology and  
107 composition were characterized by several techniques including Scanning Electron Microscopy  
108 (SEM), Energy-Dispersive X-Ray Spectroscopy (EDX), X-Ray Diffraction (XRD), carbon and  
109 oxygen elemental analyses. The effects of the material relative density and of its surface roughness  
110 on the optical properties and spectral selectivity were studied by reflectance measurements in the  
111 0.25 to 25  $\mu\text{m}$  wavelength range. The results were compared to those of pure SiC and pure TiC with  
112 various densities.

113

## 114 **2. Material and methods**

### 115 **2.1. Semi-molecular route**

116 The objective was to create an intimate mixture of the two metal oxide precursors and the carbon  
117 source during the gelling. As the precursors have a different reactivity, capping agents like  
118 carboxylic acids, acetylacetone or ethylene glycol can be used to modify the surface chemistry of the  
119 precursors and lower their reactivity [71-74]. The synthesis route is described on Figure 1 and  
120 detailed in Supplementary Information 2. Titanium isopropoxide (TTIP) and tetraethyl orthosilicate  
121 (TEOS) were chosen as the source of titanium and silicon, respectively. The system was kept under  
122 inert atmosphere by nitrogen flow to prevent unintended reactions among the raw materials and  
123 water. All additions were made dropwise under continuous stirring and heating at 90°C. Because  
124 TTIP is much more reactive than TEOS, its reactivity was first lowered by complexation with citric  
125 acid dissolved in absolute ethanol. Then, TEOS was added to the mixture, followed by sucrose  
126 dissolved into water. The co-condensation was favored by the addition of sodium fluoride. The  
127 solution was first concentrated under vacuum distillation and the resulting gel was freeze dried,  
128 grounded and sifted to produce a homogeneous powder.

129

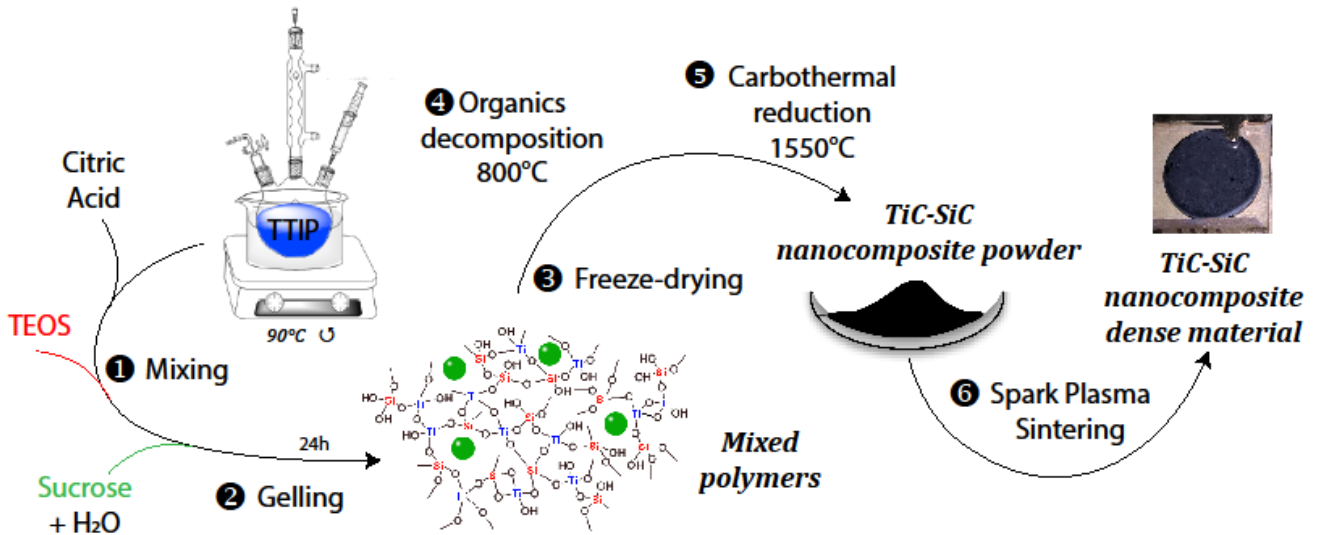
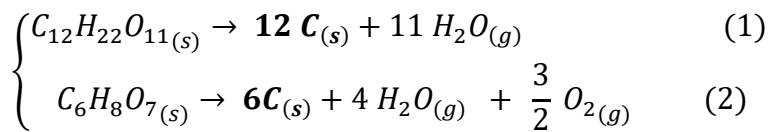


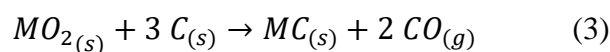
Figure 1: Reaction scheme of the synthesis route

Two heat treatments were applied under argon flow (30 L.h<sup>-1</sup>); the first one at 800°C enabled to decompose the organic parts of the precursors (sucrose and citric acid) into carbon. According to Equation (1), the decomposition of one equivalent of sucrose could provide for a maximum of 12 equivalents of carbon. However, according to the literature, the decomposition of sucrose leads to the formation of various carbon gaseous compounds (CH<sub>4</sub>, C<sub>n</sub>H<sub>2n</sub>, CO<sub>2</sub>...), leaving about 48% of efficient carbon [33]. Similarly, the decomposition of one equivalent of citric acid could provide for a maximum of 6 equivalents of carbon (Equation 2). According to several studies [75-77], after the melting of citric acid at 153°C, this compound decomposes into aconitic acid and then in citra/itaconic anhydride by dehydration and decarboxylation reactions in the range of 160-270°C. At higher temperature, several gaseous compounds are formed and the proportion of residual carbon ranges between 5 and 45%. The amount of residual carbon depends on the processing parameters, heating rate especially, but also on the complexation of citric acid with metallic element [74]. When they are mixed with the other components of the synthesis, the behavior of sucrose and citric acid may be different than when they are heated alone. The second heat treatment at 1550°C led to the carbothermal reduction of oxides into carbides according to Equation 3.

**Sucrose and citric acid decomposition -  $T = 800^{\circ}\text{C}$**



**Carbothermal reduction -  $T = 1550^{\circ}\text{C}$**



$$R = \frac{12 \cdot n_{C_{12}H_{22}O_{11}}}{3 \cdot n_{MO_2}} + \frac{6 \cdot n_{C_6H_8O_7}}{3 \cdot n_{MO_2}} \quad (4) \quad F = \frac{n_{Ti}}{n_{Ti} + n_{Si}} = \frac{n_{TTIP}}{n_{TTIP} + n_{TEOS}} = 30\% \quad (5)$$

155

156 The ratio R (Equation 4) quantifies the carbon content resulting from the decomposition of sucrose  
 157 and citric acid according to the Equations (1) and (2). Because the decomposition of sucrose and  
 158 citric acid produces not only effective carbon but also carbon gaseous species, the amount of carbon  
 159 available for the carbothermal reduction is not easily predictable and varies depending on the  
 160 conditions. The value of the R ratio leading to a stoichiometric carbothermal reaction is empirical.  
 161 According to preliminary studies, the R ratio was chosen to be 2.19 [60]. The F ratio defines the  
 162 relative proportions of Ti and Si in the final material (Equation 5). The amounts of TEOS and TTIP  
 163 used in the synthesis were adapted to produce a 30%at TiC – 70%at SiC composite, with an atomic F  
 164 ratio of 30%.

165

## 166 **2.2. Shaping**

### 167 Sintering

168 To produce materials with various densities, Spark Plasma Sintering process was used on the  
 169 composite powder resulting from the semi molecular route. Reference samples of pure TiC and pure  
 170 SiC were also made from TiC (98%) and SiC (97.5%) powders supplied by Sigma-Aldrich with an  
 171 average particle size of 3 µm and 17 µm, respectively. Sintering was conducted by Spark Plasma  
 172 Sintering apparatus (Fuji-Syntex, Dr Sinter 825, Japan) under dynamic vacuum to avoid grain  
 173 growth. A sufficient amount of powder was poured into a graphite die with an inner diameter of 20.4  
 174 mm. A compressive graphite foil (0.2 mm thick, Papyex®, Mersen Goup, France) was used as  
 175 lubricant to coat the inner surface of the die and the surface of the punches. The powder was heated  
 176 under vacuum to a maximal temperature between 1300°C to 1950°C for 5 minutes with a heating  
 177 rate of 200°C/min. The heating rate was decreased at 50°C/min the last minute of heating, to avoid  
 178 an overshoot. A uniaxial pressure of 75 MPa was applied upon heating. Cooling rate was  
 179 100°C/min. SPS is commonly used to sinter Ultra High Temperature Ceramics [78, 79].

180

### 181 Polishing

182 To produce mirror polished surfaces, the densified materials were polished with a Beta Buehler  
 183 grinder-polisher, with SiC grinding papers and with 1 µm diamond paste (Struers) according to the  
 184 procedure described in Table 1. To study the effects of surface roughness on the optical properties,  
 185 the surface of several samples was scratched with SiC grinding papers with increasing grain size, the  
 186 results of this preliminary study are given in Supplementary Information 1.

Polishing step	Grinding SiC paper		Rotation speed (rpm)	Time (min)
	Grit (grain/cm <sup>2</sup> )	Grain size (μm)		
1	1200	15.3	200	2
2	2000	10.3	200	5
3	4000	5	200	5 - 10
4	Diamond	1	200	15 - 20

Table 1: Polishing procedure.

## 2.3. Characterization methods

### Optical properties

Two spectrophotometers were used to measure the total spectral reflectance of the samples. Over the wavelength range from 0.25 to 2.5 μm, the near-normal hemispherical ( $R^{\perp,\cap}$ ) reflection spectrum was acquired with a 10 nm step using a Perkin Elmer Lambda 950 spectrophotometer. This apparatus was equipped with deuterium and tungsten lamps, PMT and InGaAs detectors, and a 150 mm integrating sphere coated with Spectralon diffuse reflective coating. The sample was illuminated at an incidence angle of 8°.

Over the wavelength range from 1.25 μm to 25 μm, the hemispherical directional reflectance ( $R^{\cap,\theta}$ ) was recorded at different detection angles  $\theta$  from 8 to 80°, using a SOC-100 HDR reflectometer (Surface Optics Corporation) coupled with a Nicolet (Fourier Transform InfraRed spectroscopy) FTIR 6700 spectrophotometer. A gold coated calibrated specular reflectance standard was used as reference during measurements (NIST calibration). The spectral range from 1.25 to 25 μm was covered by a FTIR equipped with InGaAs and DTGS/KBr detectors, coupled with Quartz and KBr beamsplitters, respectively. The sample was illuminated from all directions using a 700°C (973 K) blackbody as the infrared source and a  $2\pi$  imaging gold coated hemi ellipsoid. The light reflected by the sample at a chosen detection angle was collected by a moveable overhead mirror which directed the collimated beam into the FTIR apparatus for signal treatment to retrieve the reflectance spectrum. Each reflectance spectrum was derived from 64 consecutive scans on the same sample.

The total spectral reflectance measured and the solar spectrum were interpolated over the wavelength range from 0.25 to 25 μm with a step of 2 nm to calculate the optical parameters, using Mathematica software. The solar absorptance  $\alpha$  was calculated from room temperature measurements in the wavelength range 0.25 to 4 μm, according to Equation 6. The near-normal thermal emittance  $\varepsilon_{\theta}(T_a)$  and the hemispherical emittance  $\varepsilon_H(T_a)$  at room temperature were calculated in the wavelength range 1.25 to 25 μm according to Equations 7 and 8 respectively. The hemispherical emittance represents the propensity of a surface illuminated from all directions of the hemisphere surrounding



it to reemit radiation in the same hemisphere. As reported in the results section, at room temperature and for this type of samples, the emittance calculated from near-normal reflectance measurement is representative of the hemispherical emittance. Spectral transmittance was not measured, as the samples were opaque over the whole considered spectral range.

$$\alpha = \frac{\int_{0.25 \mu m}^{4 \mu m} [1 - R_{8^\circ}(\lambda, T_a)] \cdot G(\lambda) \cdot d\lambda}{\int_{0.25 \mu m}^{4 \mu m} G(\lambda) \cdot d\lambda} \quad (6) \quad \varepsilon_\theta(\theta, T_a) = \frac{\int_{1.25 \mu m}^{25 \mu m} [1 - R(\lambda, T_a, \theta)] \cdot P(\lambda, T_a) \cdot d\lambda}{\int_{0.25 \mu m}^{25 \mu m} P(\lambda, T_a) \cdot d\lambda} \quad (7)$$

$$\varepsilon_H(T_a) = 2 \int_0^{\pi/2} \varepsilon_\theta(\theta, T_a) \cdot \sin \theta \cdot \cos \theta \cdot d\theta \quad (8)$$

With  $\lambda$ : the wavelength [ $\mu m$ ],  $R_{8^\circ}(\lambda, T_a)$  and  $R(\lambda, T_a, \theta)$ : the spectral reflectance of the sample measured at room temperature ( $T_a$ ) with an illumination angle of  $8^\circ$  or with a variable detection angle  $\theta$ ,  $G(\lambda)$ : the standard solar irradiance spectrum (ASTM-G173 AM1.5 direct + circumsolar) [ $W \cdot m^{-2} \cdot \mu m$ ],  $P(\lambda, T_a)$ : spectral emittance (exitance) of a blackbody at room temperature derived from Planck's law [ $W \cdot m^{-2} \cdot \mu m$ ].

### Porosity, density and roughness

The apparent density ( $\rho_{app.}$ ) of the sintered samples was measured by hydrostatic weighting in pure water, using Archimedes method. Helium pycnometry measurements were conducted to determine the pycnometric density ( $\rho_{pycno.}$ ). The theoretical density ( $\rho_{th.}$ ) of the mixed carbide materials was calculated using a rule of mixtures taking into account the Si/Ti measured proportions and the amounts of free C and O. These densities were used to determine the relative density (D), the open and closed porosities ( $\phi_{open}$  and  $\phi_{closed}$ ) according to the equations reported in Supplementary Information 3.

The surface roughness of the materials was measured by means of optical interferometry (Fogale Nanotech – Microsurf 3D). This apparatus gives the global roughness of a  $287 \mu m \times 481 \mu m$  area. For each sample, a least six areas were measured to obtain an average roughness value.

### Morphology, composition and structure

The morphology of the samples was studied by Scanning Electron Microscopy (SEM), with an FEI Quanta 200 ESEM equipped with a Field Emission Gun. SEM images were recorded with back-scattered electrons (BSE) for composite samples and with secondary electrons (SE) for pure TiC and SiC samples. Energy Dispersive Spectra (EDX) were recorded using a Bruker SDD 5030 detector with a 123 eV resolution at the Mn ( $K\alpha$ ) line. EDX was used to verify the composition of the synthesized products and to study the effects of oxidation.

The global Ti/Si proportion was also measured by X-Ray Fluorescence (XRF), using a Spectro-Xepos apparatus with four secondary targets (Mo,  $Al_2O_3$ , Co and HOPG Bragg crystal).

Carbon and Oxygen analyzers (LECO CS230 and ON736) were used to measure the total carbon and oxygen contents, respectively. The samples were heated under an oxygen flow for carbon analysis or in a graphite environment for oxygen analysis. In both cases, the formation of carbon oxides was detected and quantified by infrared spectroscopy, then related to the total carbon or oxygen content in the samples. Added Fe powder was used to assist the combustion in the case of carbon analysis.

252

The samples were characterized by X-Ray Diffraction (XRD) using the Bruker D8 advance diffractometer equipped with lynxeye detector and using Cu K $\alpha$  radiation ( $\lambda=1.54184\text{\AA}$ ). Data were acquired in reflection geometry (parallel beam) in the 10-110° (2 $\theta$ ) or 10-90° (2 $\theta$ ) range of angles with steps of 0.019°. Silicon powder was collected and used as standard to evaluate the instrumental function. All the collected XRD patterns were refined by the Rietveld method with the use of the Fullprof suite package [80, 81]. TiC compound was found to crystallize in the cubic NaCl structure type in the Fm-3m space group, whereas SiC crystallizes in the ZnS structure type in the F-43m space group. During the refinement, several profile/structure parameters were allowed to vary such as zero shift, scale factor, isotropic thermal factor, unit cell parameters, moreover an anisotropic size model was applied in order to evaluate the microstructural effect. An example of the results of the Rietveld refinement obtained for the TiC compound with a relative density of 78 % is available in Supplementary Information 4.

265

### 266 3. Results

#### 267 3.1. Characterization of the final products

All the results concerning the composition and the physical shape of the samples are reported in Table 2.

Sample	Processing parameters	Composition			Sintered materials characteristics			
	T sintering (°C)	Ti/Si proportion (%mol)	C (%mass)	O (%mass)	Relative density (%)	Open porosity (%)	Closed porosity (%)	Surface roughness (nm)
TS-57	1450	31 / 69	26.6	7.2	56.6	43.4	0	52
TS-82	1550	32 / 68	25.3	5.5	81.6	16.7	1.8	20
TS-92	1650	31 / 69	26.2	6.0	92.3	6.3	1.4	13
TS-96	1750	32 / 68	26.0	5.0	95.8	1.2	3.1	10
TiC-78	1300	100 / 0	20.0	0.67	77.9	19.1	3.0	38
TiC-91	1400	100 / 0	20.7	0.56	90.5	6.9	2.6	11
TiC-94	1500	100 / 0	19.5	0.54	94.4	2.7	2.9	17
TiC-96	1700	100 / 0	19.6	0.47	95.8	1.5	2.8	15
TiC-97	1850	100 / 0	19.6	0.46	96.6	1.1	2.4	6
SiC-72	1950	0 / 100	30.4	0.20	72.1	26.5	1.4	24

270 *Table 2: Composition and measured characteristics of materials after SPS sintering for 5 min at  $P = 75\text{MPa}$  at the*  
271 *sintering temperature indicated in the table. Ti/Si proportion was obtained by average between XRF and SEM-EDX*  
272 *analyses. The theoretical %mass of C is 26 %, 20 % and 30 %, for TS composites, pure TiC and pure SiC samples,*  
273 *respectively. The error is about 0.1% for elemental analyses, relative density, and open and closed porosity. The error is*  
274 *about 1 nm for surface roughness and about 1%at for Ti/Si proportion.*

275

276 The XRF and EDX analyses reported on Supplementary Information 5 indicate a Ti / Si proportion,  
277 respectively higher and lower than the theoretical values. Nevertheless, the average values (Table 2)  
278 are close to the theoretical ones, the synthesized composites have the expected Ti / Si proportion.  
279 The amount of C globally decreases with the increase in the sintering temperature. The amount of C  
280 is close to the theoretical value (27 %, 20 % and 30 %, for TS composites, pure TiC and pure SiC  
281 samples, respectively) and the O content is higher for the composite than for the pure TiC and SiC.  
282 This high O content could be due to a insufficient amount of C available for the carboreduction after  
283 the sucrose decomposition at  $800^{\circ}\text{C}$ . Another explanation could be a too low temperature for the  
284 carboreduction, as the O content tends to decrease when the sintering temperature increases.

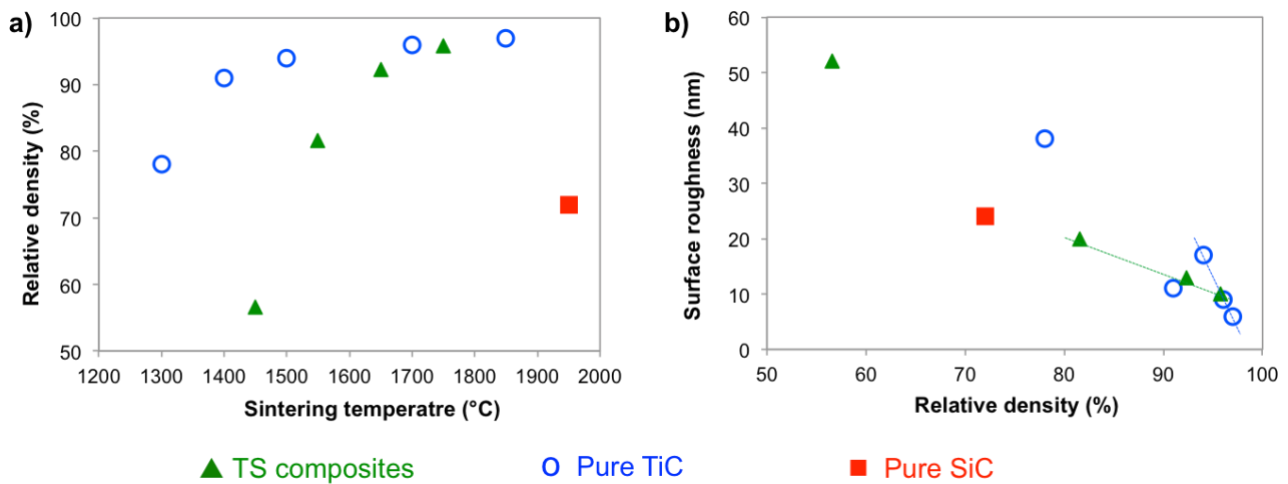
285

286 As expected, the relative density of the materials increases with the sintering temperature (Figure 2-  
287 a) [43, 82-84]. For the pure SiC sample, full relative density could not be achieved, even with a  
288 sintering temperature of  $1950^{\circ}\text{C}$ . SiC is known to be difficult to sinter because of its highly covalent  
289 bonded characteristic and the resulting low self-diffusion coefficient [85, 86].

290 For all samples, the open porosity decreases when increasing the sintering temperature and thereby  
291 with the relative density (Table 2). In the case of the composite samples, the closed porosity  
292 increases with the sintering temperature and thereby with the relative density, while it remains  
293 constant in the case of TiC samples (Table 2). During the sintering some of the open pores are  
294 closed, leading to an increase of the closed porosity.

295 The relative density of all samples appear to be correlated with the surface roughness (Figure 2-b).  
296 The evolutions are almost linear for the denser materials with the exception of sample TiC-91 which  
297 shows a surprisingly low value of surface roughness (11 nm). The slope of the curve is much higher  
298 for TS composites than for the pure TiC samples, meaning that the decrease in the relative density  
299 induces a stronger increase in surface roughness for pure TiC samples. The open porosity consists in  
300 surface holes which are partly taken into account in the value of the surface roughness.

301



302  
 303 Figure 2: a) Evolution of the relative density as a function of the sintering temperature and b) evolution of the surface  
 304 roughness as a function of the relative density. The dashed lines in b) are a guide for the eyes.

305  
 306 The morphology of the sintered materials was characterized by SEM to study the TiC and SiC grains  
 307 size and distribution (Figure 3). All composites present large areas with various electronic contrasts  
 308 due to changes in porosity and/or in composition. With the exception of sample TS-57, the electronic  
 309 contrast between the TiC grains (white) and the SiC matrix (gray) is marked (Figure 3-b to d). The  
 310 repartition of TiC grains within the SiC matrix is globally homogeneous at a short range while  
 311 presenting slight variations from one area to another. The presence of open porosity is confirmed by  
 312 SEM observation. The pore size is about 1  $\mu\text{m}$  or lower for most samples, and several microns for  
 313 the samples with the lowest densities (SiC, TS-57, TiC-78). In TS-57, it is not possible to distinguish  
 314 TiC from SiC grains, the morphology of the sample surface looks like those of non sintered powders  
 315 (see Supplementary Information 6) which could be due to the low relative density of the sample. In  
 316 all composites excepted TS-57, the TiC grains have the same size (about 150 nm). However, when  
 317 increasing the sintering temperature and thereby the relative density of the sample, the TiC grains are  
 318 brought closer, forming bigger white zones with less overall porosity.  
 319 In the case of the pure SiC sample (Figure 3-e), the grains are much bigger (about 17  $\mu\text{m}$ ) and the  
 320 open porosity is obvious. In the case of the TiC samples, the grains are smaller (about 3  $\mu\text{m}$ ) and the  
 321 decrease in open porosity is also visible in the SEM images (Figure 3-f to j).

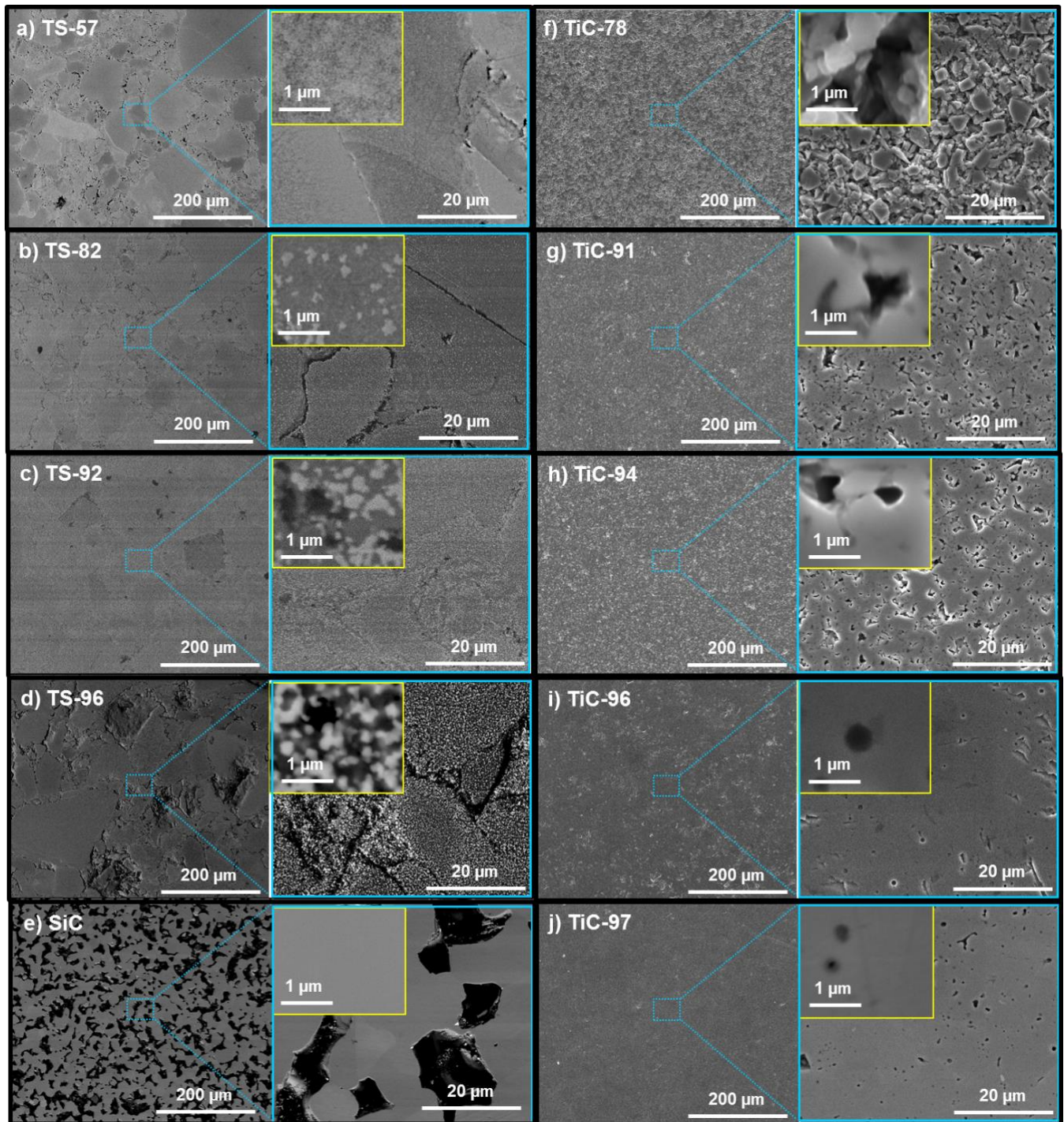


Figure 3: SEM images of the surface of the composite samples in BSE mode to show the Ti/Si distribution (a-d), the SiC reference (e) and the TiC samples (f-j) in SE mode to show the topography since there is a unique carbide phase.

After sintering, the samples were also analyzed by PXRD (Figure 4-a, b) and the results of the Rietveld refinement are presented in Figure 4-c, d) and in Table 3.

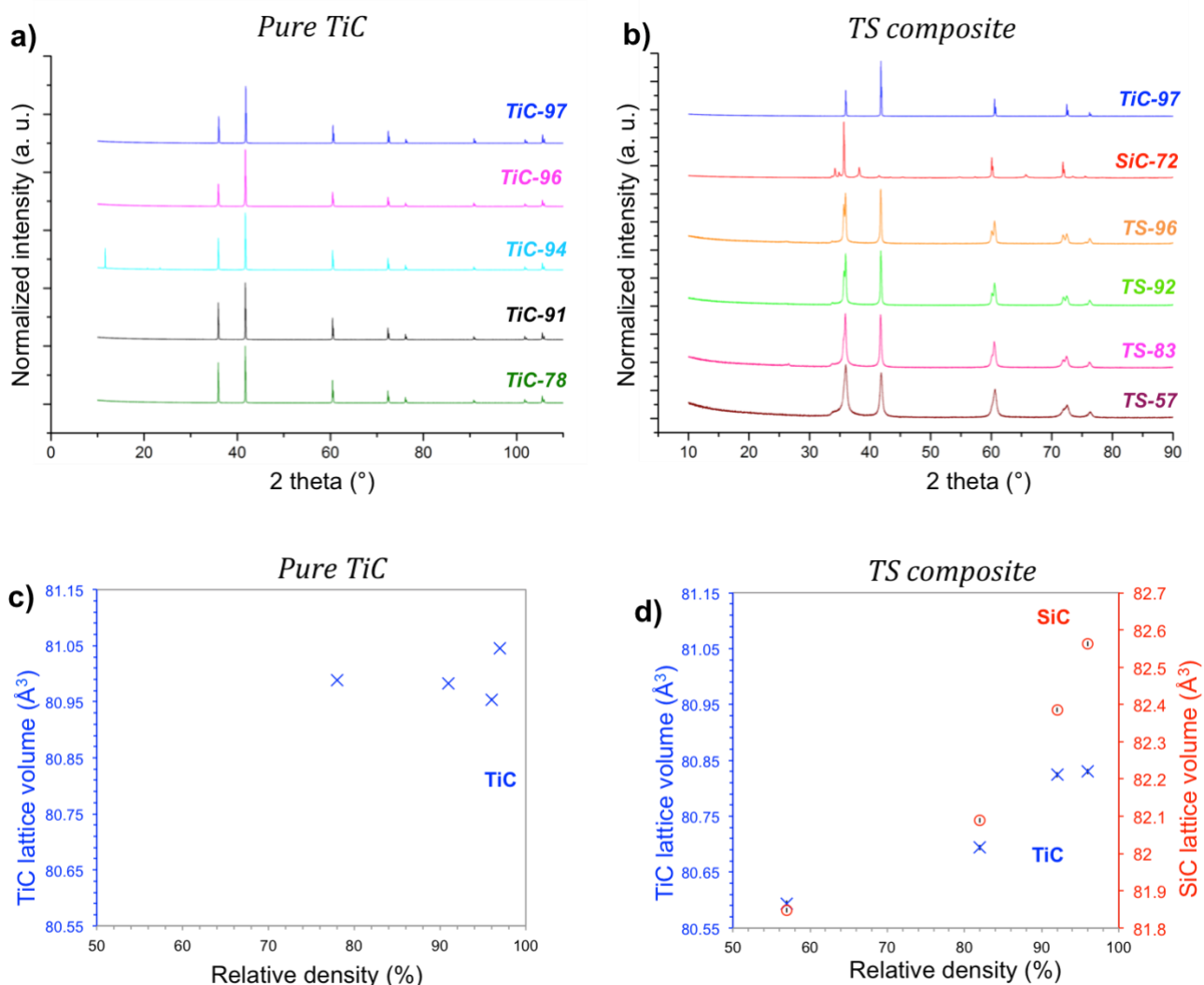
In the case of pure TiC samples, almost all the collected data showed the formation of pure and single phase. In the case of sample TiC-94, there is a reflexion around  $2\theta = 10^\circ$  which makes the Rietveld refinement impossible. From the data reported in Table 3; the obtained TiC compounds are almost free from O contamination and the O content decreases with the increase in the sintering



332 temperature. These results are in good agreement with the values determined by O elemental  
 333 analysis. The lattice volume of TiC is similar whatever the sample relative density and consistent  
 334 with the bibliography (Figure 4-c) [87]. Unfortunately, in the pure SiC sample sintered from the  
 335 commercial powder, the SiC phase crystallizes in the hexagonal system in several polymorphs which  
 336 making the Rietveld refinement impossible.

337

338 In the case of the SiC-TiC composites, both TiC and SiC cubic phases are present (Figure 4-b).  
 339 However, the possible incorporation of low amounts of Si in the TiC cubic structure (Ti or C sites)  
 340 [88] makes the Rietveld refinement complex to interpret and it was not possible to calculate precisely  
 341 the O content. The TiC and SiC unit cell parameters increase with the sintering temperature and  
 342 therefore with the sample relative density (Figure 4-d). One explanation could be the elimination of  
 343 the residual oxygen within the structure of both TiC and SiC phases as the sintering temperature  
 344 increases.



345

346 *Figure 4: a, b) X-ray diffractograms of all the samples of this study and c, d) evolution of the TiC and SiC volume*  
 347 *parameters as a function of the sample density. In c) and d), the error is about  $10^{-3} \text{\AA}^3$ .*

348

Sample	T sintering (°C)	Relative density (%)	O (%wt) elemental analysis	O (%wt) XRD	TiC lattice volume (Å <sup>3</sup> )	SiC lattice volume (Å <sup>3</sup> )
TS-57	1450	56.6	7.2	-	80.594	81.848
TS-82	1550	81.6	5.5	-	80.694	82.088
TS-92	1650	92.3	6.0	-	80.824	82.386
TS-96	1750	95.8	5.0	-	80.83	82.562
TiC-78	1300	77.9	0.67	0.69	80.988	-
TiC-91	1400	90.5	0.56	0.54	80.983	-
TiC-94	1500	94.4	0.54	-	-	-
TiC-96	1700	95.8	0.47	0.51	80.954	-
TiC-97	1850	96.6	0.46	0.15	81.045	-
SiC-72	1950	72.1	0.20	-	-	-

Table 3 : Data obtained by Rietveld refinement from PXRD measurements: TiC and SiC lattice volumes and O %wt. Comparison with the O %wt measured by elemental analysis.

### 3.2. Optical properties

To evaluate the optical properties of the samples, the total spectral reflectance was measured in the 0.25 to 25  $\mu\text{m}$  wavelength range with a near normal detection ( $8^\circ$ ) (Figure 5). It appears that the reflectance of the pure TiC samples increases with the relative density, in the whole wavelength range. The effect is small between the samples with close densities (TiC-97 to TiC-91) and more marked with the less dense sample TiC-78. The reflectance of SiC is much lower than those of TiC samples and displays the characteristic peak in the 10-14  $\mu\text{m}$  range. In the case of the TS composite, the reflectance curves are located between those of pure TiC and pure SiC and also display the SiC characteristic peak. The reflectance increases with the relative density of the sintered TS composite and the curves of the samples sintered at 1650°C and 1750°C (TS92 and TS96) are almost superimposed.

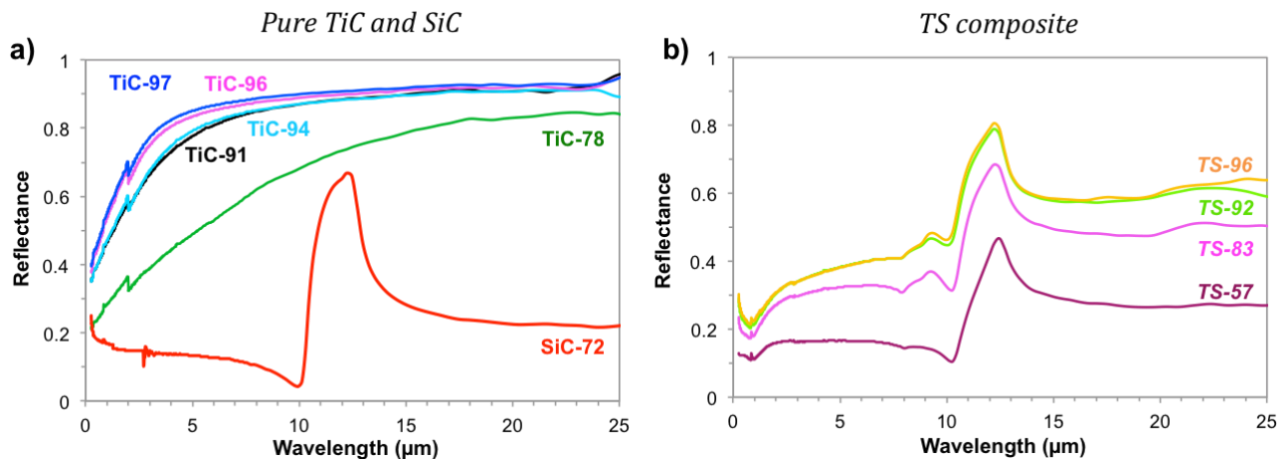


Figure 5: Evolution of the total near normal spectral reflectance for a) the pure TiC and SiC, and b) the TS composites.

## 367 4. Discussion

368

369 These materials are sought for constituting the absorber in concentrating solar power devices. In this  
370 context, they must fulfil several characteristics including good optical properties and good oxidation  
371 resistance. From the results presented above, the effects of the relative density and of the surface  
372 roughness on the optical properties are discussed below. However, the effects on the oxidation  
373 resistance were not studied here. Coulibaly et al. showed that TiC-SiC composite materials have a  
374 better oxidation resistance than pure TiC [33] and on-going work should bring new information  
375 about this topic.

376

### 377 *Effects of the sintering temperature on the material relative density, composition and structure*

378 The TiC samples on one hand, and the composite samples on the other hand, were sintered from the  
379 same powders (commercial product and synthesised by semi-molecular route, respectively) at a  
380 temperature ranging from 1300 to 1850°C. As presented in Table 2 and Figure 2, the relative density  
381 of the final material increased with the increase in the sintering temperature. Sintering did not  
382 induced the emergence of secondary phases, at least not in a sufficient amount to be detected by  
383 XRD (Figure 4). In the case of the composite, the sintering process did not modify the overall Si-Ti  
384 proportion (Table 2) or induce TiC grain growth. However, it favored their aggregation (in denser  
385 samples, TiC grains distribution is less homogeneous) (Figure 3). In addition, the increase in  
386 sintering temperature lowered the total O content in the final material which increased the volume of  
387 the TiC lattice towards the one obtained for the pure TiC samples. This increase in volume is  
388 consistent with the higher atomic radius of C compared to O. This result is in agreement with several  
389 studies about the evolution of lattice parameter of  $\text{TiC}_x\text{O}_{(1-x)}$  oxycarbide materials as a function of the  
390 composition [87, 89].

391

### 392 *Effects of the the material relative density on the optical properties*

393 For both series of samples, the reflectance increases with the increase in the relative density in the  
394 whole range of analyzed wavelengths (Figure 5). From the near-normal spectral reflectance curves,  
395 the sample total solar absorptance ( $\alpha$ ), the sample total directional and hemispherical thermal  
396 emittances ( $\epsilon_{8^\circ}$  and  $\epsilon_H$ ) have been calculated using equations (6), (7) and (8) respectively. The results  
397 are reported as a function of the sample relative density on Figure 6. As expected, the increase in the  
398 reflectance induces a decrease in both the absorptance and the emittance.

399 The values of hemispherical emittance calculated from multi-angle data (Equation 8) were almost the  
400 same as the values of directional emittance calculated from single near-normal reflectance curve  
401 (Equation 7), especially for SiC and the composite materials. The comparison is reported in



Supplementary Information 7. Therefore it can be remembered for further studies that at room temperature and for this type of samples, the emittance calculated from near-normal reflectance measurement is quite representative of the hemispherical emittance.

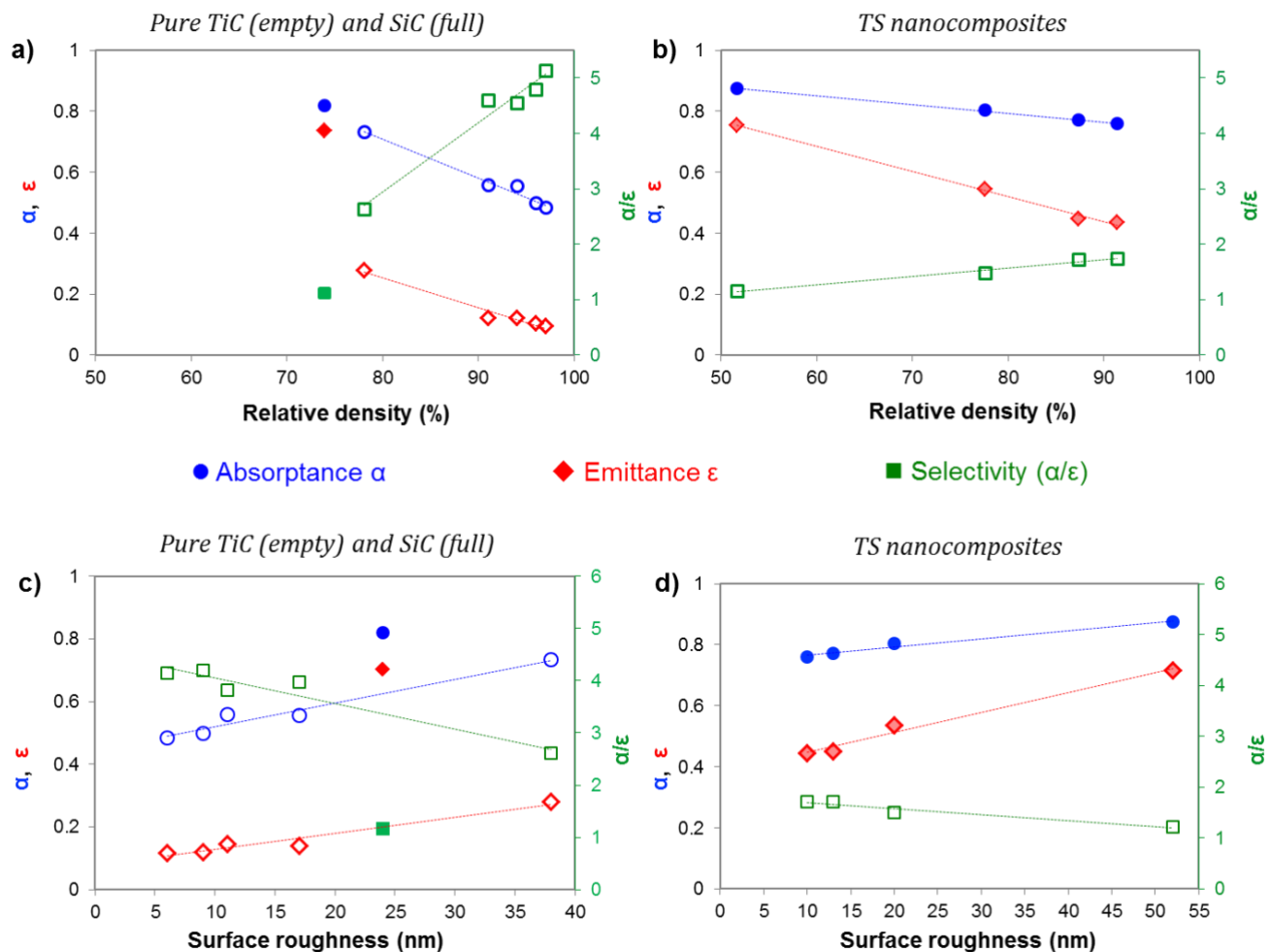


Figure 6: Evolution of the absorbance ( $\alpha$ ), the emittance ( $\epsilon$ ) and the selectivity ( $\alpha/\epsilon$ ) as a function of (a, b) the relative density and (c, d) the surface roughness of (a, c) the pure TiC and SiC samples and (b, d) the composite samples.

For all samples, the selectivity (absorbance / emittance) increases with the sample relative density (Figure 6-a, b) and decreases with the increase in surface roughness (Figure 6-c, d). These results are consistent with those of the literature and with those of our preliminary study reported in Supplementary Information 1 [19, 20, 23, 45-47]. For TS composites, the evolution of the optical properties as a function of the relative density or of the surface roughness are almost linear. The selectivity of samples TS-92 and TS-96 is the same. The increase in absorbance with surface roughness can be explained by the multi-reflexions effect: light is trapped by the walls of the surface holes and scratches. Light is reflected several times, increasing the absorbance [5, 6, 90]. The increase in emittance is related to the increase in specific surface area as the surface roughness increases. By definition, the quantity of energy emitted by a material is proportional to its surface.

420 When comparing with the pure SiC and pure TiC references (Figure 6-a), it appears that all  
421 nanocomposite samples (Figure 6-b) have a higher selectivity than the pure SiC reference but lower  
422 than the one of the pure TiC reference. Due to their good spectral selectivity, these nanocomposite  
423 materials could therefore be good candidates for bulk solar applications, especially the denser ones.  
424 As TS-92 and TS-96 samples have the same value of spectral selectivity, we could consider that a  
425 SPS sintering temperature of 1650°C is sufficient to obtain a composite with interesting optical  
426 properties.

427

428 One can wonder if the effect of the sample relative density on its optical properties is only a surface  
429 effect or if the bulk has to be considered. There is a tight link between relative density and surface  
430 roughness, especially for the composite samples (Figure 2-c-d).

431 In the case of the composite, the two denser samples (TS-92 and TS-96) have the same spectral  
432 selectivity, their reflectance curves are almost superimposed despite a difference in relative density  
433 of 4 % and a difference in surface roughness of 3 nm. In the case of the three denser TiC samples  
434 (TiC-94, TiC-96, TiC-97), the difference in relative density is similar (3 %) but the difference in  
435 surface roughness is much higher (7 nm), as well as the effects on the optical properties. Therefore,  
436 the effects on the optical properties seems to be mainly due to changes in surface roughness, at least  
437 for samples with a relative density higher than 90 %.

438

439 To thoroughly determine whether the closed porosity has an impact on the optical properties, the  
440 emittance should be measured directly from the non-illuminated face of the samples and not  
441 calculated from the surface reflectance curve [11]. On going work should bring new information  
442 about this question.

443 The key to increase the spectral selectivity is to increase the absorptance without increasing the  
444 emittance. Several ideas have been proposed in the literature, among them, the concept of directional  
445 selectivity. As the incident solar radiation is directional while the radiative losses are hemispherical,  
446 an optical cavity can be used to trap the incident solar radiation and reflect the emitted radiation back  
447 to the absorber [91]. Similarly, Hollands et al. proposed to use corrugated specular surfaces to  
448 selectively absorb the directional solar radiation while limiting the hemispherical radiation losses  
449 [50]. It could also be interesting to extend the study to higher frequencies, and monitor the properties  
450 of the SiC-TiC composites as electromagnetic wave absorber as it has been done for SiC/Si<sub>3</sub>N  
451 composites [92, 93].

452

453

454

## 455 **Conclusion**

456 In this paper the potential of SiC-TiC nanocomposite materials for bulk solar absorber applications  
457 was studied. 70%at SiC – 30%at TiC nanocomposite materials were successfully synthesized by a  
458 sol-gel route from alkoxides as metal oxide precursors and sucrose as the carbon source. The  
459 carbothermal reduction was conducted at relatively low temperature (1550°C) compared to the  
460 conventional process. The resulting powder was composed of nanometric TiC and SiC particles  
461 homogeneously mixed, with 5-7 %wt of residual O. The sintering process was then adapted to  
462 produce compacts with various densities. Reference materials of pure TiC with increasing densities  
463 were also sintered from commercial TiC powder.

464 The spectral reflectance was measured in the 0.25 to 25  $\mu\text{m}$  wavelength range to evaluate the spectral  
465 selectivity of these materials. The effects of the sample relative density and surface roughness were  
466 studied and their correlation was discussed. A tight link between the sample relative density and its  
467 surface roughness was identified and explained by considering the open porosity as the main  
468 contribution to surface roughness. The reflectance was found to increase in the whole wavelength  
469 range, with the increase in relative density and the decrease in surface roughness. Therefore, the  
470 denser and smoother the sample, the higher its spectral selectivity. The TiC-SiC composite had an  
471 intermediate reflectance compared to the pure SiC and the pure TiC samples. With an absorptance of  
472 0.76, an emittance of 0.44 and a selectivity of 1.74, the denser SiC-TiC could be a good candidate for  
473 bulk solar applications. Even though these values are slightly lower than those obtained for other  
474 materials like  $\text{ZrB}_2$ , HfC or TaC, it should be recalled that these materials also have to be resistant to  
475 oxidation which is the case of our SiC-TiC composite [21, 33, 94]. In addition, several solutions  
476 from the literature were proposed to improve these optical properties by increasing the absorptance  
477 while maintaining a low emittance.

478

## 479 **Acknowledgments**

480 This work was funded by the RBPCH project from the Nuclear Energy Division of CEA and by the  
481 National Agency for Research (ANR) of the French State in the framework of the CARAPASS  
482 project (award n°ANR-16-CE08-0026) and of the French "Investments for the future" programme  
483 managed by ANR under contracts ANR-10-LABX-22-01-SOLSTICE and ANR-10-EQPX-49-  
484 SOCRATE. We wish to thank Renaud Podor and Joseph Lautru for SEM imaging, Bruno Corso for  
485 XRD assistance, Cyrielle Rey for helium pycnometry measurements and furnace assistance and  
486 Christophe Escape for his help in reflectometry measurements.

487

## 488 **Declarations of interest**

489 The authors declare no competing interests.

## 490 References

- 491 [1] C.G. Granqvist, Solar energy materials, *Advanced Materials* 15(21) (2003) 1789-1803.
- 492 [2] Y. Tian, C.Y. Zhao, A review of solar collectors and thermal energy storage in solar thermal  
493 applications, *Applied Energy* 104 (2013) 538-553.
- 494 [3] J. Spitz, Selective surfaces for high-temperature solar photothermal conversion, *Thin Solid Films*  
495 45(1) (1977) 31-41.
- 496 [4] J. Spitz, D. Mazierebezes, Selective materials for solar-energy photothermal conversion, *Journal*  
497 *of Optics-Nouvelle Revue D Optique* 15(5) (1984) 325-332.
- 498 [5] W.F. Bogaerts, C.M. Lampert, Materials for photothermal solar-energy conversion, *Journal of*  
499 *Materials Science* 18(10) (1983) 2847-2875.
- 500 [6] C.M. Lampert, Coatings for enhanced photo thermal energy collection .1. Selective absorbers,  
501 *Solar Energy Materials* 1(5-6) (1979) 319-341.
- 502 [7] C.C. Agrafiotis, I. Mavroidis, A.G. Konstandopoulos, B. Hoffschmidt, P. Stobbe, M. Romero, V.  
503 Fernandez-Quero, Evaluation of porous silicon carbide monolithic honeycombs as volumetric  
504 receivers/collectors of concentrated solar radiation, *Solar Energy Materials and Solar Cells* 91(6)  
505 (2007) 474-488.
- 506 [8] E. Sani, L. Mercatelli, D. Jafrancesco, J.L. Sans, D. Sciti, Ultra-High Temperature Ceramics for  
507 solar receivers: spectral and high-temperature emittance characterization, *Journal of the European*  
508 *Optical Society-Rapid Publications* 7 (2012).
- 509 [9] H.H. Blau, J.R. Jasperse, Spectral emittance of refractory materials, *Applied Optics* 3(2) (1964)  
510 281-&.
- 511 [10] L. Mercatelli, M. Meucci, E. Sani, Design and test of a new facility for assessing spectral  
512 normal emittance of solid materials at high temperature, in: S. Jiang, M.J.F. Digonnet (Eds.), *Optical*  
513 *Components and Materials Xiii*2016.
- 514 [11] L. Mercatelli, M. Meucci, E. Sani, Facility for assessing spectral normal emittance of solid  
515 materials at high temperature, *Applied Optics* 54(29) (2015) 8700-8705.
- 516 [12] E. Sani, L. Mercatelli, J.L. Sans, D. Sciti, Optical properties of black and white ZrO<sub>2</sub> for solar  
517 receiver applications, *Solar Energy Materials and Solar Cells* 140 (2015) 477-482.
- 518 [13] E. Sani, M. Meucci, L. Mercatelli, D. Jafrancesco, J.L. Sans, L. Silvestroni, D. Sciti, Optical  
519 properties of boride ultrahigh-temperature ceramics for solar thermal absorbers, *Journal of Photonics*  
520 *for Energy* 4 (2014).
- 521 [14] D. Sciti, L. Silvestroni, J.L. Sans, L. Mercatelli, M. Meucci, E. Sani, Tantalum diboride-based  
522 ceramics for bulk solar absorbers, *Solar Energy Materials and Solar Cells* 130 (2014) 208-216.
- 523 [15] E. Sani, L. Mercatelli, J.L. Sans, L. Silvestroni, D. Sciti, Porous and dense hafnium and  
524 zirconium ultra-high temperature ceramics for solar receivers, *Optical Materials* 36(2) (2013) 163-  
525 168.
- 526 [16] D. Sciti, L. Silvestroni, L. Mercatelli, J.L. Sans, E. Sani, Suitability of ultra-refractory diboride  
527 ceramics as absorbers for solar energy applications, *Solar Energy Materials and Solar Cells* 109  
528 (2013) 8-16.
- 529 [17] E. Sani, L. Mercatelli, D. Fontani, J.L. Sans, D. Sciti, Hafnium and tantalum carbides for high  
530 temperature solar receivers, *Journal of Renewable and Sustainable Energy* 3(6) (2011).
- 531 [18] E. Sani, L. Mercatelli, F. Francini, J.L. Sans, D. Sciti, Ultra-refractory ceramics for high-  
532 temperature solar absorbers, *Scripta Materialia* 65(9) (2011) 775-778.
- 533 [19] L. Mercatelli, E. Sani, D. Jafrancesco, P. Sansoni, D. Fontani, M. Meucci, S. Coraggia, L.  
534 Marconi, J.L. Sans, E. Beche, L. Silvestroni, D. Sciti, Ultra-refractory diboride ceramics for solar  
535 plant receivers, *Proceedings of the Solarpaces 2013 International Conference* 49 (2014) 468-477.
- 536 [20] E. Sani, L. Mercatelli, M. Meucci, A. Balbo, L. Silvestroni, D. Sciti, Compositional dependence  
537 of optical properties of zirconium, hafnium and tantalum carbides for solar absorber  
538 applications *Solar Energy* - 131(-) (2016) - 207.
- 539 [21] E. Sani, L. Mercatelli, M. Meucci, A. Balbo, C. Musa, R. Licheri, R. Orru, G. Cao, Optical  
540 properties of dense zirconium and tantalum diborides for solar thermal absorbers, *Renewable Energy*  
541 91 (2016) 340-346.

542 [22] E. Sani, E. Landi, D. Sciti, V. Medri, Optical properties of ZrB<sub>2</sub> porous architectures, *Solar*  
543 *Energy Materials and Solar Cells* 144 (2016) 608-615.

544 [23] E. Sani, L. Mercatelli, M. Meucci, L. Silvestroni, A. Balbo, D. Sciti, Process and composition  
545 dependence of optical properties of zirconium, hafnium and tantalum borides for solar receiver  
546 applications, *Solar Energy Materials and Solar Cells* 155 (2016) 368-377.

547 [24] E. Sani, M. Meucci, L. Mercatelli, A. Balbo, C. Musa, R. Licheri, R. Orru, G. Cao, Titanium  
548 diboride ceramics for solar thermal absorbers, *Solar Energy Materials and Solar Cells* 169 (2017)  
549 313-319.

550 [25] L. Charpentier, M. Balat-Pichelin, D. Sciti, L. Silvestroni, High temperature oxidation of Zr-  
551 and Hf-carbides: Influence of matrix and sintering additive, *Journal of the European Ceramic Society*  
552 33(15-16) (2013) 2867-2878.

553 [26] L. Charpentier, M. Balat-Pichelin, E. Beche, D. Sciti, L. Silvestroni, Microstructural  
554 characterization of ZrC-MoSi<sub>2</sub> composites oxidized in air at high temperatures, *Applied Surface*  
555 *Science* 283 (2013) 751-758.

556 [27] A. Onuma, H. Kiyono, S. Shimada, M. Desmaison, High temperature oxidation of sintered TiC  
557 in an H<sub>2</sub>O-containing atmosphere, *Solid State Ionics* 172(1-4) (2004) 417-419.

558 [28] S. Shimada, A thermoanalytical study on the oxidation of ZrC and HfC powders with formation  
559 of carbon, *Solid State Ionics* 149(3-4) (2002) 319-326.

560 [29] S. Shimada, K. Mochidsuki, The oxidation of TiC in dry oxygen, wet oxygen, and water vapor,  
561 *Journal of Materials Science* 39(2) (2004) 581-586.

562 [30] M. Gherrab, V. Garnier, S. Gavarini, N. Millard-Pinard, S. Cardinal, Oxidation behavior of  
563 nano-scaled and micron-scaled TiC powders under air, *International Journal of Refractory Metals &*  
564 *Hard Materials* 41 (2013) 590-596.

565 [31] J. Sempere, R. Nomen, E. Serra, B. Sempere, D. Guglielmi, Thermal behavior of oxidation of  
566 TiN and TiC nanoparticles, *Journal of Thermal Analysis and Calorimetry* 105(2) (2011) 719-726.

567 [32] V.V. Rudneva, G.V. Galevskii, Investigation of thermal oxidation resistance of nanopowders of  
568 refractory carbides and borides, *Russian Journal of Non-Ferrous Metals* 48(2) (2007) 143-147.

569 [33] M. Coulibaly, G. Arrachart, A. Mesbah, X. Deschanel, From colloidal precursors to metal  
570 carbides nanocomposites MC (M=Ti, Zr, Hf and Si): Synthesis, characterization and optical spectral  
571 selectivity studies, *Solar Energy Materials and Solar Cells* 143 (2015) 473-479.

572 [34] J. Cabrero, F. Audubert, R. Pailler, Fabrication and characterization of sintered TiC-SiC  
573 composites, *Journal of the European Ceramic Society* 31(3) (2011) 313-320.

574 [35] J. Chen, W.J. Li, W. Jiang, Characterization of sintered TiC-SiC composites, *Ceramics*  
575 *International* 35(8) (2009) 3125-3129.

576 [36] K.S. Cho, Y.W. Kim, H.J. Choi, J.G. Lee, In situ-toughened silicon carbide-titanium carbide  
577 composites, *Journal of the American Ceramic Society* 79(6) (1996) 1711-1713.

578 [37] H. Endo, M. Ueki, H. Kubo, Hot-pressing of SiC-TiC composites, *Journal of Materials Science*  
579 25(5) (1990) 2503-2506.

580 [38] H. Endo, M. Ueki, H. Kubo, Microstructure and mechanical-properties of hot-pressed SiC-TiC  
581 composites, *Journal of Materials Science* 26(14) (1991) 3769-3774.

582 [39] Y.M. Luo, S.Q. Li, P. Wei, L. Liu, Fabrication and mechanical evaluation of SiC-TiC  
583 nanocomposites by SPS, *Materials Letters* 58(1-2) (2004) 150-153.

584 [40] D. Shaoming, J. Dongliang, T. Shouhong, G. Jingkun, Mechanical properties of SiC/TiC  
585 composites by hot isostatic pressing, *Journal of Materials Science Letters* 15(5) (1996) 394-396.

586 [41] G.C. Wei, P.F. Becher, Improvements in mechanical-properties in SiC by the addition of TiC  
587 particles, *Journal of the American Ceramic Society* 67(8) (1984) 571-574.

588 [42] M.A. Janney, Microstructural development and mechanical-properties of SiC and SiC-TiC  
589 composites, *American Ceramic Society Bulletin* 65(2) (1986) 357-362.

590 [43] L.J. Wang, W. Jiang, L.D. Chen, S.Q. Bai, Rapid reactive synthesis and sintering of submicron  
591 TiC/SiC composites through spark plasma sintering, *Journal of the American Ceramic Society* 87(6)  
592 (2004) 1157-1160.

593 [44] M. Khodaei, O. Yaghobizadeh, H.R. Baharvandi, A. Dashti, Effects of different sintering  
594 methods on the properties of SiC-TiC, SiC-TiB<sub>2</sub> composites, *International Journal of Refractory*  
595 *Metals & Hard Materials* 70 (2018) 19-31.

596 [45] D. Sciti, L. Silvestroni, L. Mercatelli, J.-L. Sans, E. Sani, Suitability of ultra-refractory diboride  
597 ceramics as absorbers for solar energy applications, *Solar Energy Materials and Solar Cells* 109  
598 (2013) 8-16.

599 [46] D. Sciti, L. Silvestroni, J.-L. Sans, L. Mercatelli, M. Meucci, E. Sani, Tantalum diboride-based  
600 ceramics for bulk solar absorbers, *Solar Energy Materials and Solar Cells* 130 (2014) 208-216.

601 [47] E. Sani, L. Mercatelli, M. Meucci, L. Zoli, D. Sciti, Lanthanum hexaboride for solar energy  
602 applications, *Scientific Reports* 7 (2017).

603 [48] D. Sciti, L. Silvestroni, D.M. Trucchi, E. Cappelli, S. Orlando, E. Sani, Femtosecond laser  
604 treatments to tailor the optical properties of hafnium carbide for solar applications, *Solar Energy*  
605 *Materials and Solar Cells* 132 (2015) 460-466.

606 [49] D. Sciti, D.M. Trucchi, A. Bellucci, S. Orlando, L. Zoli, E. Sani, Effect of surface texturing by  
607 femtosecond laser on tantalum carbide ceramics for solar receiver applications, *Solar Energy*  
608 *Materials and Solar Cells* 161 (2017) 1-6.

609 [50] K.G.T. Hollands, Directional selectivity, emittance and absorptance properties of even corrugated  
610 specular surfaces, *Solar Energy* 7(3) (1963) 108-116.

611 [51] E.G. Acheson, Manufacture of graphite, Google Patents, 1896.

612 [52] N.A. Hassine, J.G.P. Binner, T.E. Cross, Synthesis of refractory-metal carbide powders via  
613 microwave carbothermal reduction, *International Journal of Refractory Metals & Hard Materials*  
614 13(6) (1995) 353-358.

615 [53] M.D. Sacks, C.A. Wang, Z.H. Yang, A. Jain, Carbothermal reduction synthesis of  
616 nanocrystalline zirconium carbide and hafnium carbide powders using solution-derived precursors,  
617 *Journal of Materials Science* 39(19) (2004) 6057-6066.

618 [54] V.M. Kevorkijan, M. Komac, D. Kolar, Low-temperature synthesis of sinterable SiC powders  
619 by carbothermic reduction of colloidal SiO<sub>2</sub>, *Journal of Materials Science* 27(10) (1992) 2705-2712.

620 [55] Y.J. Lin, C.P. Tsang, The effects of starting precursors on the carbothermal synthesis of SiC  
621 powders, *Ceramics International* 29(1) (2003) 69-75.

622 [56] H.P. Martin, R. Ecke, E. Muller, Synthesis of nanocrystalline silicon carbide powder by  
623 carbothermal reduction, *Journal of the European Ceramic Society* 18(12) (1998) 1737-1742.

624 [57] A. Julbe, A. Larbot, C. Guizard, L. Cot, J. Charpin, P. Bergez, Effect of boric-acid addition in  
625 colloidal sol-gel derived SiC precursors, *Materials Research Bulletin* 25(5) (1990) 601-609.

626 [58] V.D. Krstic, Production of fine, high-purity beta silicon-carbide powders, *Journal of the*  
627 *American Ceramic Society* 75(1) (1992) 170-174.

628 [59] X. Deschanel, D. Herault, G. Arrachart, C. Rey, A. Grandjean, G. Toquer, R. Podor, T. Zemb,  
629 G. Cerveau, R. Corriu, Comparison of two soft chemistry routes for the synthesis of mesoporous  
630 carbon/beta-SiC nanocomposites, *Journal of Materials Science* 48(11) (2013) 4097-4108.

631 [60] M. Coulibaly, Carbures nanocomposites issus de précurseurs sol-gel et impacts sur la sélectivité  
632 optique Montpellier, 2015.

633 [61] K. Thorne, S.J. Ting, C.J. Chu, J.D. Mackenzie, T.D. Getman, M.F. Hawthorne, Synthesis of  
634 TiC via polymeric titanates - the preparation of fibres and thin-films, *Journal of Materials Science*  
635 27(16) (1992) 4406-4414.

636 [62] P. Gupta, W. Wang, L.S. Fan, Synthesis of high-surface-area SiC through a modified Sol-Gel  
637 route: Control of the pore structure, *Industrial & Engineering Chemistry Research* 43(16) (2004)  
638 4732-4739.

639 [63] S.M. El-Sheikh, Z.I. Zaki, Y.M.Z. Ahmed, In situ synthesis of ZrC/SiC nanocomposite via  
640 carbothermic reduction of binary xerogel, *Journal of Alloys and Compounds* 613 (2014) 379-386.

641 [64] J. Zhong, S.Q. Liang, K. Wang, H.T. Wang, T. Williams, H. Huang, Y.B. Cheng, Synthesis of  
642 Mesoporous Carbon-Bonded TiC/SiC Composites by Direct Carbothermal Reduction of Sol-Gel  
643 Derived Monolithic Precursor, *Journal of the American Ceramic Society* 94(11) (2011) 4025-4031.

644 [65] H. Zhang, F. Li, Q. Jia, G. Ye, Preparation of titanium carbide powders by sol-gel and  
645 microwave carbothermal reduction methods at low temperature, *Journal of Sol-Gel Science and*  
646 *Technology* 46(2) (2008) 217-222.

647 [66] R. Corriu, P. Gerbier, C. Guerin, B. Henner, The thermal-conversion of poly(silylene)-  
648 diacetylene metal-oxide composites - A new approach to beta-SiC-MC ceramics, *Angewandte*  
649 *Chemie-International Edition in English* 31(9) (1992) 1195-1197.

650 [67] R.J.P. Corriu, *Ceramics and nanostructures from molecular precursors*, *Angewandte Chemie-*  
651 *International Edition* 39(8) (2000) 1376-1398.

652 [68] R.J.P. Corriu, P. Gerbier, C. Guerin, B. Henner, From preceramic polymers with  
653 interpenetrating networks to SiC/MC nanocomposites, *Chemistry of Materials* 12(3) (2000) 805-811.

654 [69] X. Deschanel, M. El Ghazzal, C. Delchet, D. Herauld, V. Magnin, A. Grandjean, R. Podor, G.  
655 Cerveau, T. Zemb, R. Corriu, Synthesis of carbide compounds derived from colloidal oxide and  
656 carbohydrate, in: S. Bucak (Ed.), *Trends in Colloid and Interface Science Xxiii2010*, pp. 47-52.

657 [70] S.T. Bae, H. Shin, H.S. Jung, K.S. Hong, Synthesis of Titanium Carbide Nanoparticles with a  
658 High Specific Surface Area from a TiO<sub>2</sub> Core-Sucrose Shell Precursor, *Journal of the American*  
659 *Ceramic Society* 92(11) (2009) 2512-2516.

660 [71] C. Ang, T. Williams, A. Seeber, H.T. Wang, Y.B. Cheng, Synthesis and Evolution of Zirconium  
661 Carbide via SolGel Route: Features of Nanoparticle OxideCarbon Reactions, *Journal of the*  
662 *American Ceramic Society* 96(4) (2013) 1099-1106.

663 [72] D. Hanaor, M. Michelazzi, C. Leonelli, C.C. Sorrell, The effects of carboxylic acids on the  
664 aqueous dispersion and electrophoretic deposition of ZrO<sub>2</sub>, *Journal of the European Ceramic Society*  
665 32(1) (2012) 235-244.

666 [73] S. Mahata, B. Mondal, S.S. Mahata, K. Usha, N. Mandal, K. Mukherjee, Chemical modification  
667 of titanium isopropoxide for producing stable dispersion of titania nano-particles, *Materials*  
668 *Chemistry and Physics* 151 (2015) 267-274.

669 [74] I.A. Mudunkotuwa, V.H. Grassian, Citric Acid Adsorption on TiO<sub>2</sub> Nanoparticles in Aqueous  
670 Suspensions at Acidic and Circumneutral pH: Surface Coverage, Surface Speciation, and Its Impact  
671 on Nanoparticle-Nanoparticle Interactions, *Journal of the American Chemical Society* 132(42)  
672 (2010) 14986-14994.

673 [75] M.M. Barbooti, D.A. Alsammerrai, Thermal-decomposition of citric-acid, *Thermochimica Acta*  
674 98 (1986) 119-126.

675 [76] D. Wyrzykowski, E. Hebanowska, G. Nowak-Wicz, M. Makowski, L. Chmurzynski, Thermal  
676 behaviour of citric acid and isomeric aconitic acids, *Journal of Thermal Analysis and Calorimetry*  
677 104(2) (2011) 731-735.

678 [77] T. Sadik, C. Pillon, C. Carrot, J.A.R. Ruiz, Dsc studies on the decomposition of chemical  
679 blowing agents based on citric acid and sodium bicarbonate, *Thermochimica Acta* 659 (2018) 74-81.

680 [78] R. Belon, G. Antou, N. Pradeilles, A. Maitre, D. Gosset, Mechanical behaviour at high  
681 temperature of spark plasma sintered boron carbide ceramics, *Ceramics International* 43(8) (2017)  
682 6631-6635.

683 [79] G. Antou, N. Pradeilles, M. Gendre, A. Maitre, New approach of the evolution of densification  
684 mechanisms during Spark Plasma Sintering: Application to zirconium (oxy-)carbide ceramics,  
685 *Scripta Materialia* 101 (2015) 103-106.

686 [80] T. Roisnel, J. Rodriguez-Carvajal, WinPLOTR: A Windows tool for powder diffraction pattern  
687 analysis, *European Powder Diffraction*, Pts 1 and 2 378-3 (2001) 118-123.

688 [81] J. Rodriguez-Carvajal, Recent advances in magnetic-structure determination by neutron powder  
689 diffraction, *Physica B* 192(1-2) (1993) 55-69.

690 [82] M. Mashhadi, H. Khaksari, S. Safi, Pressureless sintering behavior and mechanical properties of  
691 ZrB<sub>2</sub>-SiC composites: effect of SiC content and particle size, *Journal of Materials Research and*  
692 *Technology-Jmr&T* 4(4) (2015) 416-422.

693 [83] M. Mashhadi, M. Shambuli, S. Safi, Effect of MoSi<sub>2</sub> addition and particle size of SiC on  
694 pressureless sintering behavior and mechanical properties of ZrB<sub>2</sub>-SiC-MoSi<sub>2</sub> composites, *Journal*  
695 *of Materials Research and Technology-Jmr&T* 5(3) (2016) 200-205.

696 [84] P. Barick, D. Chakravarty, B.P. Saha, R. Mitra, S.V. Joshi, Effect of pressure and temperature  
697 on densification, microstructure and mechanical properties of spark plasma sintered silicon carbide  
698 processed with beta-silicon carbide nanopowder and sintering additives, *Ceramics International*  
699 42(3) (2016) 3836-3848.

700 [85] N.Z. Khalil, S.K. Vajpai, M. Ota, K. Ameyama, Effect of Particle Size Distribution on SiC  
701 Ceramic Sinterability, *Materials Transactions* 56(11) (2015) 1827-1833.

702 [86] A. Lara, A.L. Ortiz, A. Munoz, A. Dominguez-Rodriguez, Densification of additive-free  
703 polycrystalline beta-SiC by spark-plasma sintering, *Ceramics International* 38(1) (2012) 45-53.

704 [87] B. Jiang, N. Hou, S. Huang, G. Zhou, J. Hou, Z. Cao, H. Zhu, Structural studies of  $TiC_{1-x}O_x$   
705 solid solution by Rietveld refinement and first-principles calculations, *Journal of Solid State*  
706 *Chemistry* 204 (2013) 1-8.

707 [88] O. Tengstrand, N. Nedfors, B. Alling, U. Jansson, A. Flink, P. Eklund, L. Hultman,  
708 Incorporation effects of Si in  $TiC_x$  thin films, *Surface & Coatings Technology* 258 (2014) 392-397.

709 [89] F. Réjasse, O. Rapaud, J. L  chelle, G. Trolliard, H. Khodja, O. Masson, G. Martin, A. Ma  tre,  
710 Novel insight into the chemical analysis of light elements in oxycarbides, *Acta materialia* 157 (2018)  
711 11-20.

712 [90] G. Pellegrini, Experimental methods for the preparation of selectively absorbing textured  
713 surfaces for photo thermal solar conversion, *Solar Energy Materials* 3(3) (1980) 391-404.

714 [91] L. Weinstein, D. Kraemer, K. McEnaney, G. Chen, Optical cavity for improved performance of  
715 solar receivers in solar-thermal systems, *Solar Energy* 108 (2014) 69-79.

716 [92] P. Wang, L.F. Cheng, Y.N. Zhang, L.T. Zhang, Flexible SiC/Si<sub>3</sub>N<sub>4</sub> Composite Nanofibers with  
717 in Situ Embedded Graphite for Highly Efficient Electromagnetic Wave Absorption, *Acs Applied*  
718 *Materials & Interfaces* 9(34) (2017) 28844-28858.

719 [93] P. Wang, L.F. Cheng, L.T. Zhang, One-dimensional carbon/SiC nanocomposites with tunable  
720 dielectric and broadband electromagnetic wave absorption properties, *Carbon* 125 (2017) 207-220.

721 [94] E. Sani, L. Mercatelli, M. Meucci, A. Balbo, L. Silvestroni, D. Sciti, Compositional dependence  
722 of optical properties of zirconium, hafnium and tantalum carbides for solar absorber applications,  
723 *Solar Energy* 131 (2016) 199-207.

724